Electronic Supplementary Material (ESI) for Inorganic Chemistry Frontiers.

Electronic Supplementary Information

Promoting formation of oxygen vacancies in ceria multishelled hollow microspheres by doping iron for enhanced ambient ammonia electrosynthesis

Cha Li,[a] Mengmeng Wang,[a] Liping Ren[a] and Hongming Sun*[a]

[a] College of Chemistry, Tianjin Key Laboratory of Structure and Performance for Functional Molecules, Tianjin Normal University, Tianjin 300387, China

* Corresponding author. E-mail: hxxyshm@tjnu.edu.cn

Contents

1. Experimental section

Material: Sodium hydroxide (NaOH, 96%) was purchased from Tianjin Kermel Chemical Reagent Co., Ltd. Hydrochloric acid (HCl, 36~38%) was purchased from Tianjin Fengchuan Chemical Reagent Co., Ltd. Ethanol (AR), Isopropanol(AR), sodium sulfate (99%), and ammonium chloride (NH_4Cl, 99%) were purchased from Tianjin Damao Chemical Trading Co., Ltd. Sodium nitroprusside ($C_5H_4FeN_6Na_2O_3$, 99%) and salicylic acid ($C_7H_6O_3$, 99.5%) were purchased from Ron Reagent. Hydrazine hydrate (N_2H_4, 5% HCl) was obtained from Guobiao (Beijing) Testing and Certification, Co., Ltd. NaClO (6~14% active chlorine basis), Cerium (III) nitrate hexahydrate ($Ce(NO_3)_3$, 99.95%) was obtained from Maclin. Urea (CH_4N_2O, 99.5%), D-(+)-Glucose ($C_6H_{12}O_6$, 99.5%), trisodium citrate dihydrate ($C_6H_5Na_3O_7$, 98%), p-dimethylaminobenzaldehyde ($C_9H_{11}NO$, 98%) and Ammonium chloride-^{15}N($^{15}NH_4Cl$, 98.5%) were purchased from Aladdin Industrual. Ferric Nitrate Nonahydrate($Fe(NO_3)_3 \bullet 9H_2O$, 99%) was purchased from Nine-Dinn chemistry (shanghai) Co., Ltd. $^{14}N_2$ gas (99.999%) and Ar gas (99.999%) were obtained from Huanyu Co., Ltd. $^{15}N_2$ gas (99.99%) was obtained from Tianjin Taiya Co., Ltd. All chemicals were used as received without further purification.

Synthesis of CeO_2 HM and Fe-CeO_2 HM

The preparation of multishelled Fe-CeO_2 HM can be divided into three steps: synthesis of carbon sphere/Ce/Fe compound, annealing the carbon sphere/Ce/Fe compound in air to form multishelled Fe-CeO_2 hollow microsphere precursor, and then annealing the precursor in hydrogen and argon mixture (H_2/Ar = 1/9) to form Fe-CeO_2 HM with oxygen vacancies. Typically, 5.4 g glucose ($C_6H_{12}O_6 \cdot H_2O$), 0.56 g urea ($CO(NH_2)_2$), 0.1529 g $Fe(NO_3)_3 \cdot 9H_2O$ and 0.1644 g $Ce(NO_3)_3 \cdot 6H_2O$ were dissolved in 70 mL deionized water with adequate stirring at room temperature. Then, the mixed solution was transferred into Teflon-lined stainless steel autoclave (100 mL) and reacted at 160 °C for 16 h. After the reaction, the solution was naturally cooled to room temperature, and the black-brown precipitate in the autoclave was collected. Subsequently, the black-brown precipitate washed with distilled water and ethanol for several times, and dried at 60 °C for 12 h. The obtained black-brown powder was calcined in air at 550 °C for 4 h, forming multishelled Fe-CeO_2 hollow microsphere precursor (abbreviated as Fe-CeO_2 HM-Precursor). For generating oxygen vacancies, the multishelled Fe-CeO_2 hollow microsphere precursor was further calcined at 200 °C under hydrogen and argon mixture (H_2/Ar = 1/9) atmosphere for 0.5 h, obtaining the multishelled Fe-CeO_2 hollow microspheres (Fe-CeO_2 HM) with rich oxygen vacancies. The pure CeO_2 HM, Fe_2O_3 HM and Fe doped CeO_2 HM sample with other Fe doping mass content were synthesised using same synthesis method.

For comparison, Fe-CeO_2 nanorods were also prepared by a previously reported method[1]. Typically, 1.644 g $Ce(NO_3)_3 \cdot 6H_2O$ and 0.217 g $Fe(NO_3)_3 \cdot 9H_2O$ and were dissolved in 20 mL deionized water to form solution A. Then, 20 g NaOH was dissolved in 60 mL deionized water to form solution B. Solution B was quickly injected into solution A and kept vigorous stirring for 0.5 h. Then, the mixed slurry was transferred into Teflon-lined stainless steel autoclave (100 mL) and reacted at 90 °C for 24 h. After cooling down to room temperature, the precipitate was collected by centrifugation and washed with distilled water and ethanol for several times, and dried at 60 °C for 12 h. The obtained powder was calcined in air at 550 °C for 4 h, and then calcined at 200 °C under hydrogen and argon mixture (H_2/Ar = 1/9) atmosphere for 0.5 h to form Fe-CeO_2 nanorods.

2. Characterization of materials

The powder XRD pattern was gained on a Rigaku model Ultima IV diffractometer with a Rigaku D/teX ultra-high-speed position-sensitive detector and Cu-Kα X-ray (40 kV and 100 mA) to identify the crystalline structures. The SEM image was examined on the FEI Nova Nano 230 scanning electron microscope. The energy of the electron beam was 15 and 20 keV, respectively. TEM imaging was performed on a Philips Tecnai F20 system at 200 kV. The chemical composition and valence state of the sample were tested by XPS (AXIS ULTRA AlKα1486.6 eV). The element composition was also passed ICP-AES (PerkinElmerBest 83000). The porosity was measured on a BELSORP-Mini instrument with a 77 K nitrogen adsorption-desorption isotherm. Furthermore, the instruments and excitations were taken for Raman spectra characterization are Lab Ram Aramis Raman and HeeNe laser (λ = 633 nm), respectively. Mapada UV 6300 spectrophotometer (Shanghai, China) was taken for detect UV-Vis absorbance. ^1H NMR spectra were recorded on a

Bruker NMR spectrometer (400 MHz) with chemical shifts reported as ppm in DMSO-d6.

3. Preparations of the working electrodes

First, 7 mg of Fe-CeO_2 HM powder mixed with 3 mg carbon (Vulcan XC-72) were dispersed in 950 μL of isopropanol containing 50 μL of Nafion, and a uniform suspension was formed after ultrasonic treatment for 1 h. Then, the suspension was droped onto a glassy carbon electrode (0.07065 cm^2) with a total mass load of 0.283 mg/cm^2. The electrode was used as a working electrode for electrochemical test.

4. Electrocatalytic measurements

The electrochemical measurements were conducted on a CHI model 760E electrochemical workstation using an airtight typical three-electrode H-cell separated by a Nafion 117 membrane (DuPont) at room temperature and pressure. A platinum electrode and a SCE were used as the counter and reference electrode, respectively. In this work, the real value of measured potential (E_{SCE}) for a SCE electrode versus the reversible hydrogen electrode (RHE) was standardized using a platinum plate electrode (1 × 1 cm^2) to test the H_2 evolution and oxidation polarization curves in hydrogen atmosphere at a scan rate 5 mV s^{-1}. The electrolyte was 0.1 M anhydrous sodium sulfate (Na_2SO_4). N_2 and Ar gases were pretreated severally by flowing into 0.1 M KOH and 0.1 M H_2SO_4 water solutions, ensuring no N-containing impurity in the gases for NRR tests. Before each electrochemical measurement, the electrochemical system was bubbled continuously with N_2 gas for more than 30 min, and the gas was maintained throughout the reactions. The scan rate of linear scan voltammetry is set to 1 mV s^{-1}, and the current density is normalized by the geometric surface area. The NRR performance of the catalyst was tested for 2 h using the potentiostatic method at room temperature.

5. Ammonia quantification by Nessler's reagent method and indophenol blue method

The detection of NH_3 was made by ultraviolet spectrophotometry using indophenol blue method and Nessler's reagent method.[2,3] For Nessler's reagent method, 300 μL potassium sodium tartrate solution (0.2 M) was added into 3 mL post-electrolysis electrolyte. Subsequently, 300 μL Nessler's reagent was mixed with the resulting solution. The mixture was kept in dark for 20 min. Finally, the absorption spectra of the obtained solution at λ = 425 nm was tested by ultraviolet-visible (UV-vis) spectrophotometer. To calculate the amount of produced NH_3, the calibration curve was fitted using standard ammonia chloride solutions of 0.01, 0.03, 0.05, 0.07, 0.09, 0.1, 0.15, 0.20, 0.25 and 0.30 mM in 0.1 M Na_2SO_4. The fitting curve (y =2.0751 x + 0.0077, R^2 = 0.9997) shows good linear relation of absorbance value with NH_3 concentration by three times independent calibrations. For the indophenol blue method, 1 mL of the post-electrolysis electrolyte was pipetted and mixed with 1 M NaOH solution containing 5 wt% salicylic acid and 5 wt% sodium citrate. Then, 500 μL NaClO solution (0.05 M) and 100 μL sodium nitroferricyanide solution (1 wt%) were added into the mixture sequentially. After 2 h, the mixed solution was tested by ultraviolet-visible (UV-vis) spectrophotometer to obtain the absorption spectra and the peak of the resulting indophenol blue was at λ = 655 nm. To calculate the amount of produced NH_3, the calibration curve was fitted using standard ammonia chloride solutions of 0, 0.1, 0.25, 0.5, 1 and 2 μg mL^{-1} in 0.1 M Na_2SO_4. The fitting curve (y = 0.517 x + 0.0364, R^2 = 0.9993) shows good linear relation of absorbance value with NH_3 concentration by three times independent calibrations.

6. Calculations of NH_3 yield and Faradic efficiency (FE)

The ammonia yield and FE can be calculated according to Eq. (1), Eq. (2)

$$NH_3\ yield = 17 \times c(NH_3) \times V \div (m \times t) \quad (1)$$

$$FE = 3 \times F \times c(NH_3) \times V \div (17 \times Q) \quad (2)$$

where $c(NH_3)$ is the NH_3 concentration, V is the electrolyte volume, t is the electrolysis time, m is the catalyst weight, F is Faraday constant (96485 C mol^{-1}) and Q is the total charge during electrolysis.

7. Hydrazine quantification

The hydrazine concentration was estimated by the method of Watt and Chrisp.[4] A mixture of p-dimethylaminobenzaldehyde (4 g), concentrated hydrochloric acid (20 mL) and ethanol (200

mL) was used as a color reagent. 5 mL electrolyte taken out from the cathodic chamber was added into 5 mL color reagent. After 15 min, the absorbance of the resulting solution was measured at 455 nm by using UV-vis spectrophotometer. The yield of N_2H_4 were estimated from a concentration-absorbance calibration curve using standard hydrazine monohydrate solution of 0.000, 0.001, 0.003, 0.005, 0.007, 0.009, 0.010 and 0.015 mM in 0.1 M Na_2SO_4. The fitting curve ($y = 35.782x + 0.0262, R^2 = 0.9992$) shows good linear relation of absorbance with N_2H_4 concentration by three times of independent calibrations.

8. Isotope labeling experiment

The ^{14}N and ^{15}N isotopic experiments were conducted using $^{14}N_2$ and $^{15}N_2$ as feeding gases for nitrogen reduction catalysis. Prior to use for NRR tests, $^{14}N_2$ and $^{15}N_2$ gases were purged through 1 mM H_2SO_4 solution and water to eliminate the potential contaminants. After 2 h electrochemical NRR in 0.1 M Na_2SO_4 solution at –0.4 V vs RHE, the post electrolyte solution was concentrated to 2.0 mL. Then, this solution was mixed with HCl and DMSO-d6 solutions and used for ^1H NMR measurement (Bruker AVANCE AV III 400).

9. Figures and tables

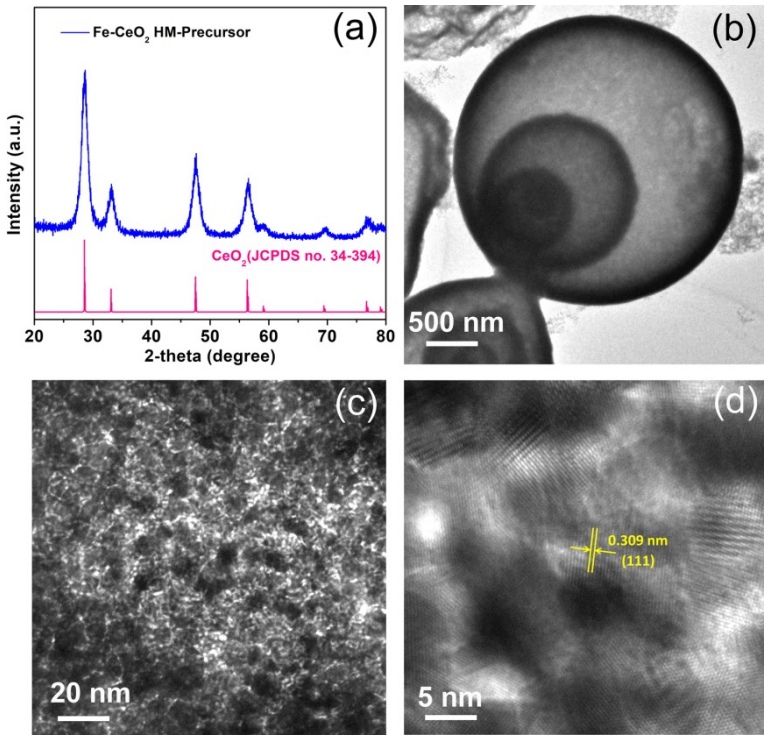

Fig. S1 (a) XRD pattern (b-d) Low- and high-magnification TEM images of Fe-CeO_2 HM-Precursor only calcined in air.

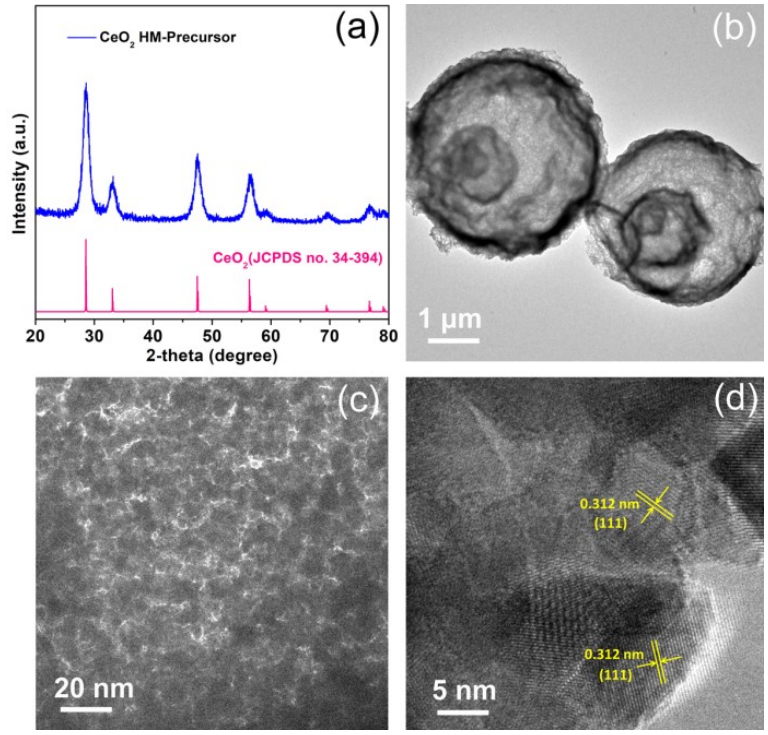

Fig. S2 (a) XRD pattern, (b-d) Low- and high-magnification TEM images of CeO_2 HM-Precursor only calcined in air.

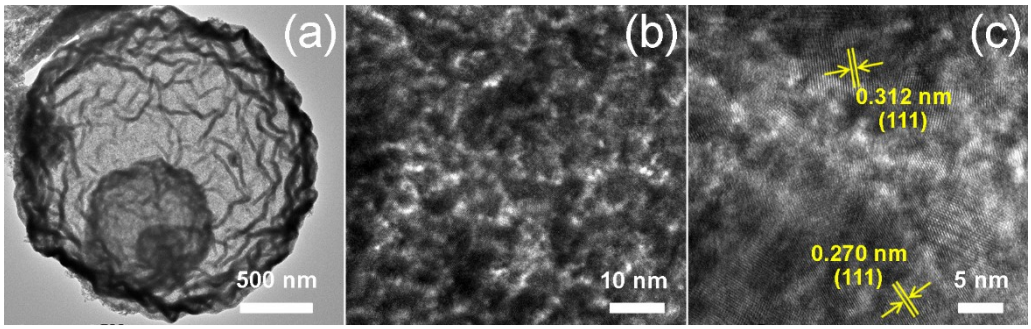

Fig. S3 TEM (a) and HRTEM (b, c) image of CeO_2 HM

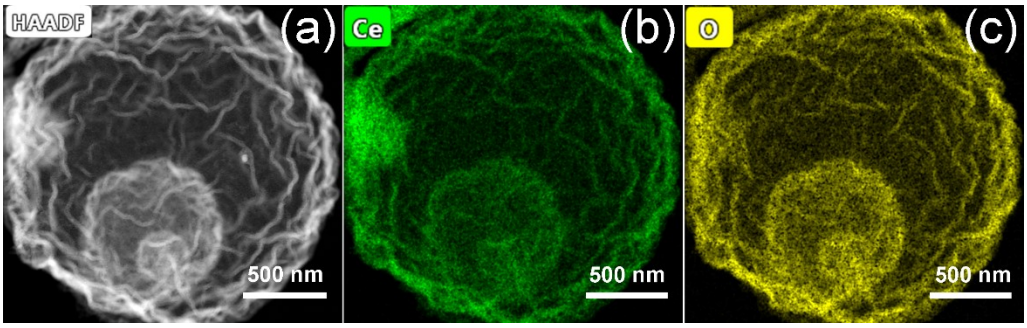

Fig. S4 HAADF-STEM image and STEM-EDS elemental mapping of CeO_2 HM

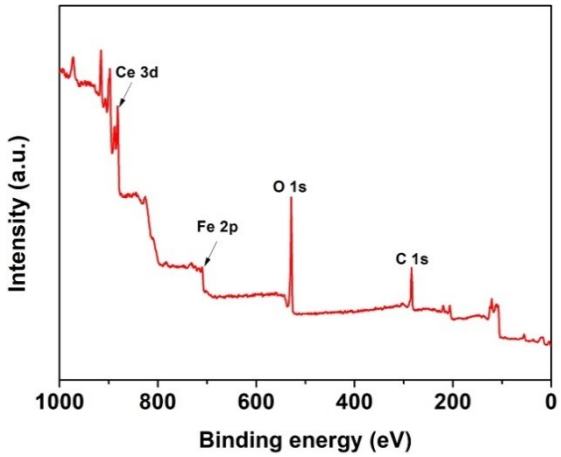

Fig. S5 The surface survey XPS spectra of Fe-CeO_2 HM

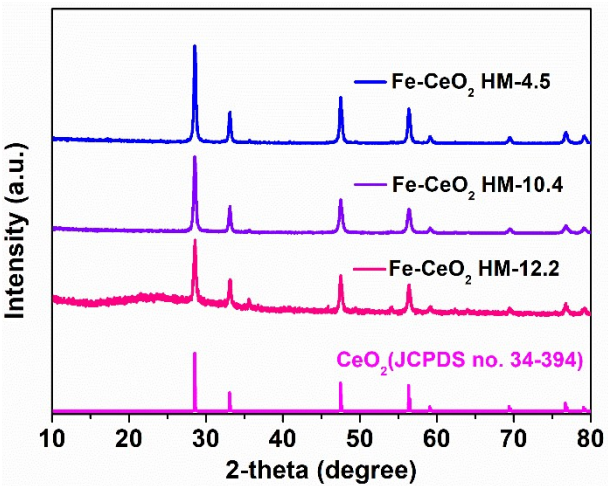

Fig. S6 XRD pattern of Fe doped CeO_2 catalysts with different Fe doping mass content.

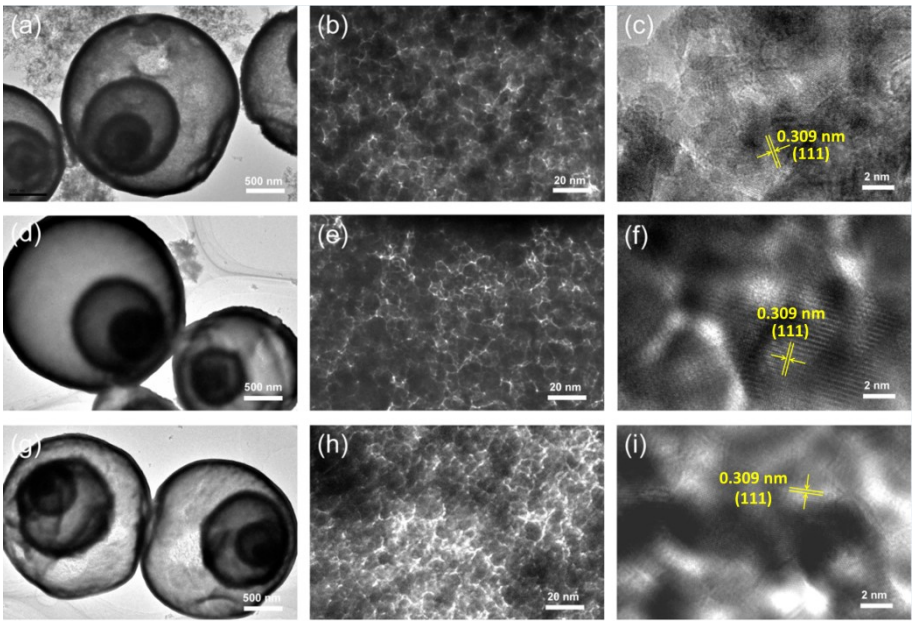

Fig. S7 TEM and HRTEM image of (a-c) CeO_2 HM-4.5, (d-f) CeO_2 HM-10.4 and (g-i) CeO_2 HM-12.2.

Table S1 The doped Fe content in different samples determined by ICP–AES

Catalyst	Fe (mg)	Fe (μmol)	Mass Content (wt.%)
Fe-CeO_2 HM-4.5	0.225	4.017	4.5
Fe-CeO_2 HM-7.1	0.355	6.339	7.1
Fe-CeO_2 HM-10.4	0.520	9.285	10.4
Fe-CeO_2 HM-12.2	0.610	10.892	12.2

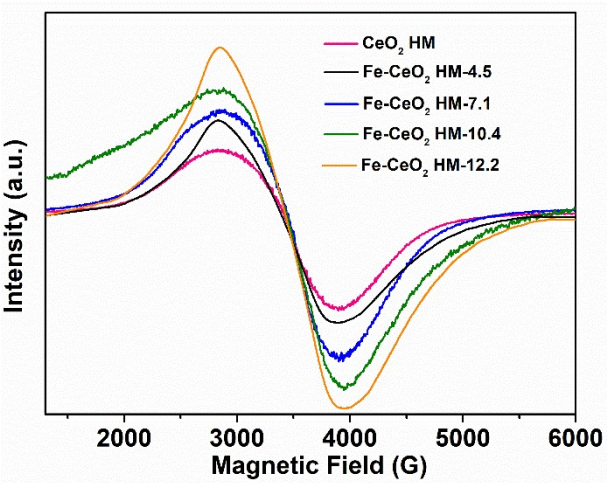

Fig. S8 Electron paramagnetic resonance (EPR) spectra of CeO_2 HM, Fe-CeO_2 HM-4.5, Fe-CeO_2 HM-7.1, Fe-CeO_2 HM-10.4, Fe-CeO_2 HM-12.2

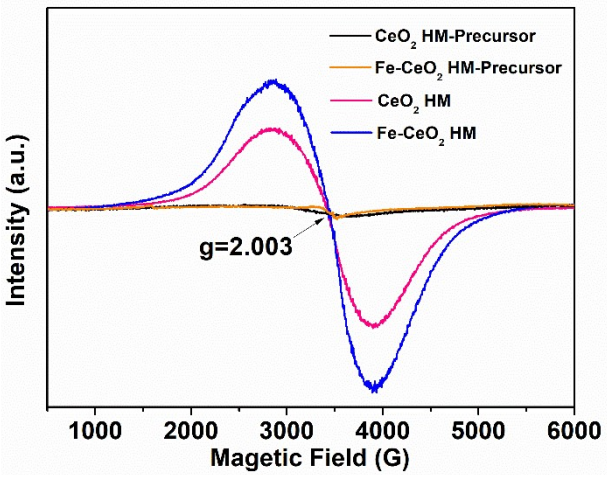

Fig. S9 Electron paramagnetic resonance (EPR) spectra of CeO_2 HM-Precursor and Fe-CeO_2 HM-Precursor only calcined in air, as well as CeO_2 HM and Fe-CeO_2 HM samples.

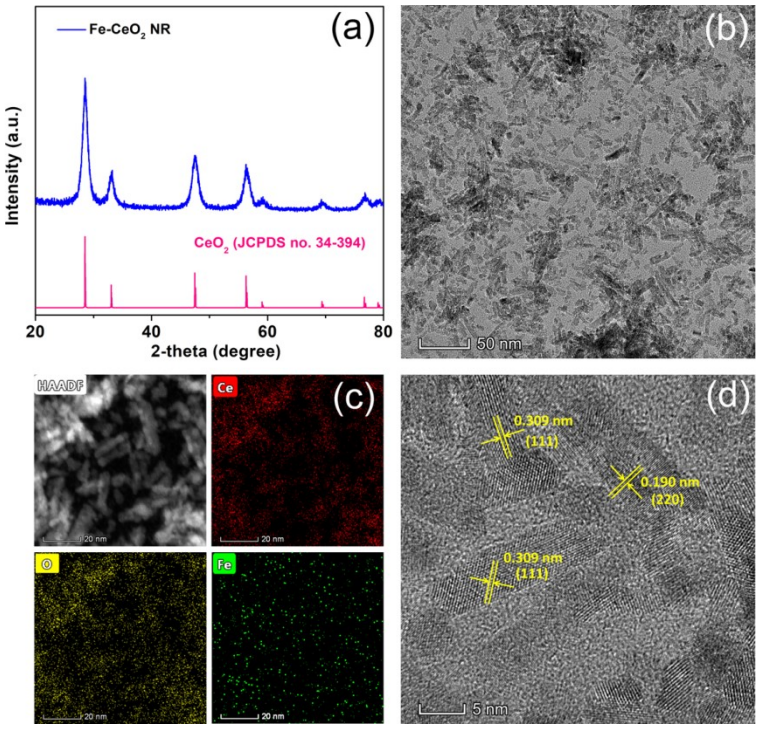

Fig. S10 (a) XRD pattern, (b) TEM image, (c) EDS elemental mapping images and (d) high-magnification TEM image of Fe-CeO_2 nanorods (abbreviated as Fe-CeO_2 NR).

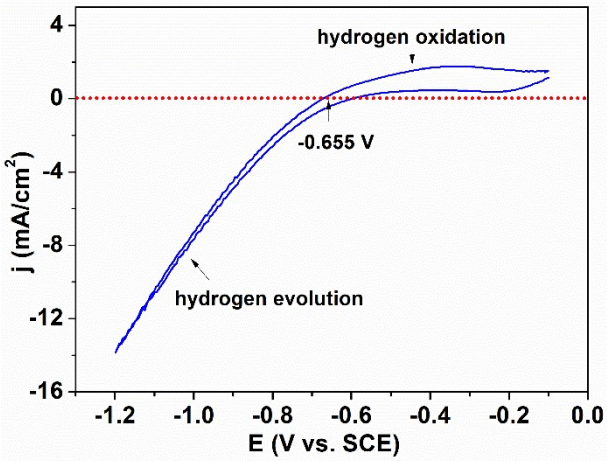

Fig. S11 Potential calibration of reference electrode in H_2-saturated 1.0 M Na_2SO_4 solution. CV curves of platinum plate electrode recorded at a scan rate 5 mV s^{-1}. The CV result of RHE calibration: $E_{(RHE)} = E_{(SCE)} + 0.655\,V$.

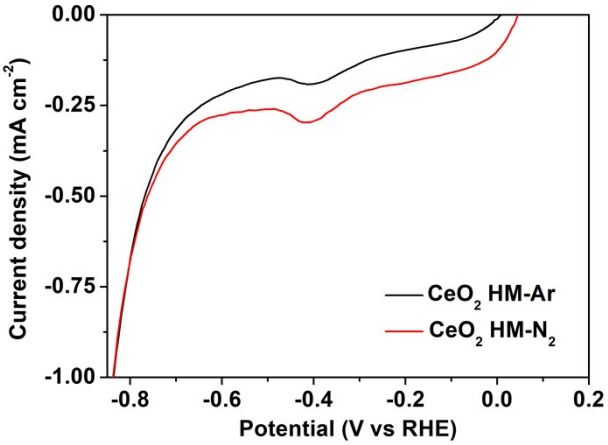

Fig. S12. Polarization curves of CeO_2 HM.

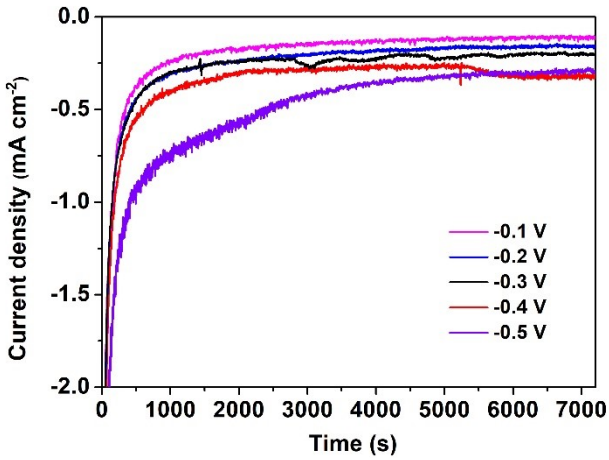

Fig. S13 Chronoamperometry curves of CeO_2 HM catalyst obtained at different potentials in N_2-saturated 0.1 M Na_2SO_4 solution.

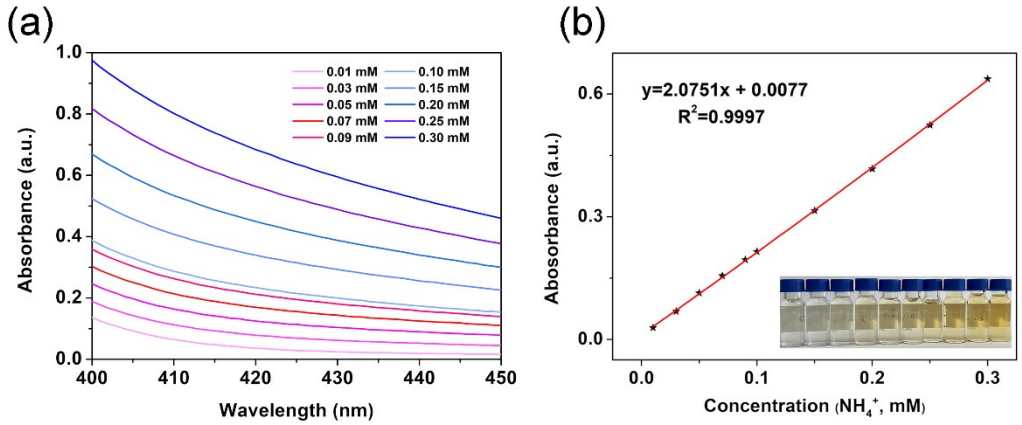

Fig. S14 (a) UV-vis curves of Nessler's reagent solutions. (b) Calibration curve used to estimate the concentrations of NH_4^+ ions.

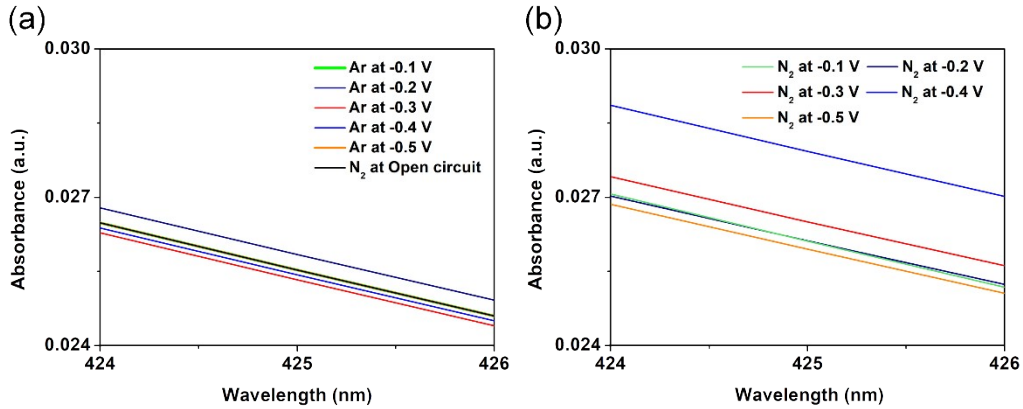

Fig. S15 (a) UV-vis colorimetric spectra of Ar-saturated electrolytes stained by Nessler indicator after 2 h electrolysis at respective potentials and N_2-saturated electrolytes stained by Nessler indicator after 2 h electrolysis under open circuit potential. (b) UV-vis colorimetric spectra N_2-saturated electrolytes stained by Nessler indicator after 2 h electrolysis at respective potentials.

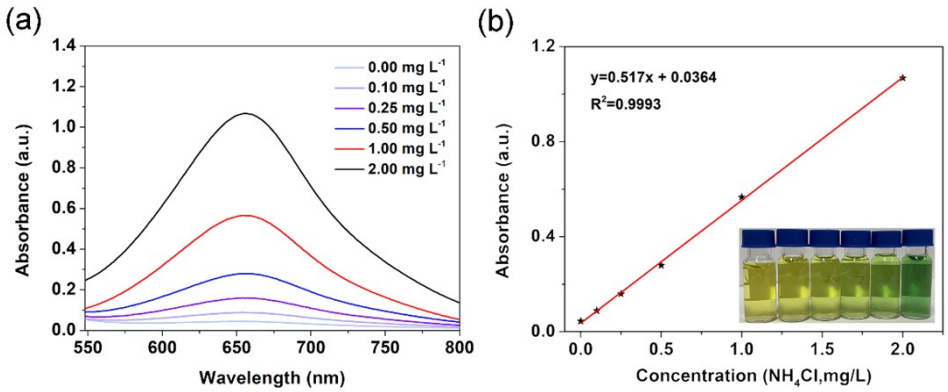

Fig. S16 (a) UV-vis colorimetric spectra of indophenol blue solutions. (b) Calibration curve used to estimate the concentrations of NH_4^+ ions.

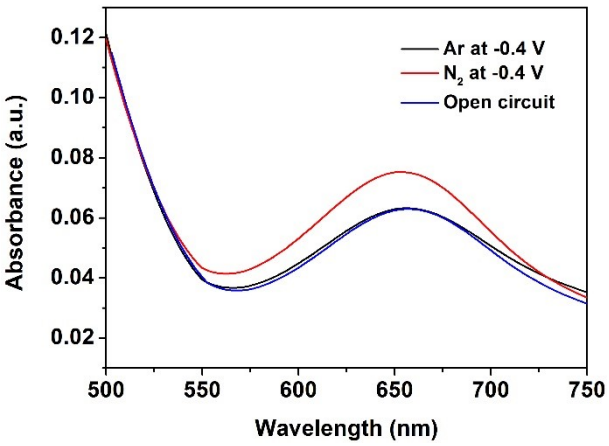

Fig. S17 UV-vis colorimetric spectra of Ar-saturated electrolyte stained by indophenol blue indicator after 2 h electrolysis by Fe-CeO_2 HM modified electrode under a potential of –0.4 V (black), N_2-saturated electrolyte stained by indophenol blue indicator after 2 h electrolysis by Fe-CeO_2 HM modified electrode under –0.4 V (red) and N_2-saturated electrolytes stained by indophenol blue indicator after 2 h electrolysis by Fe-CeO_2 HM modified electrode under open circuit potential (blue).

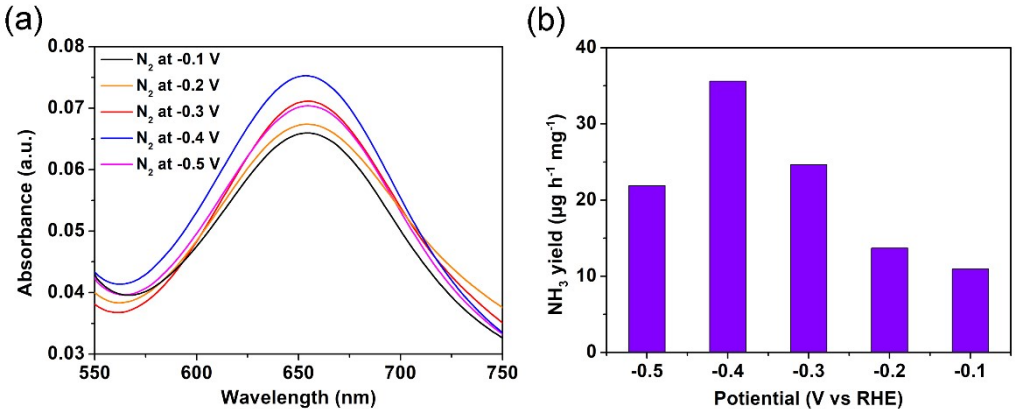

Fig. S18 (a) UV-vis colorimetric spectra of N_2-saturated electrolyte stained by indophenol blue indicator after 2 h electrolysis by Fe-CeO_2 HM modified electrode under at respective potentials. (b) The comparison of NH_3 yield detected by indophenol blue method at different potentials.

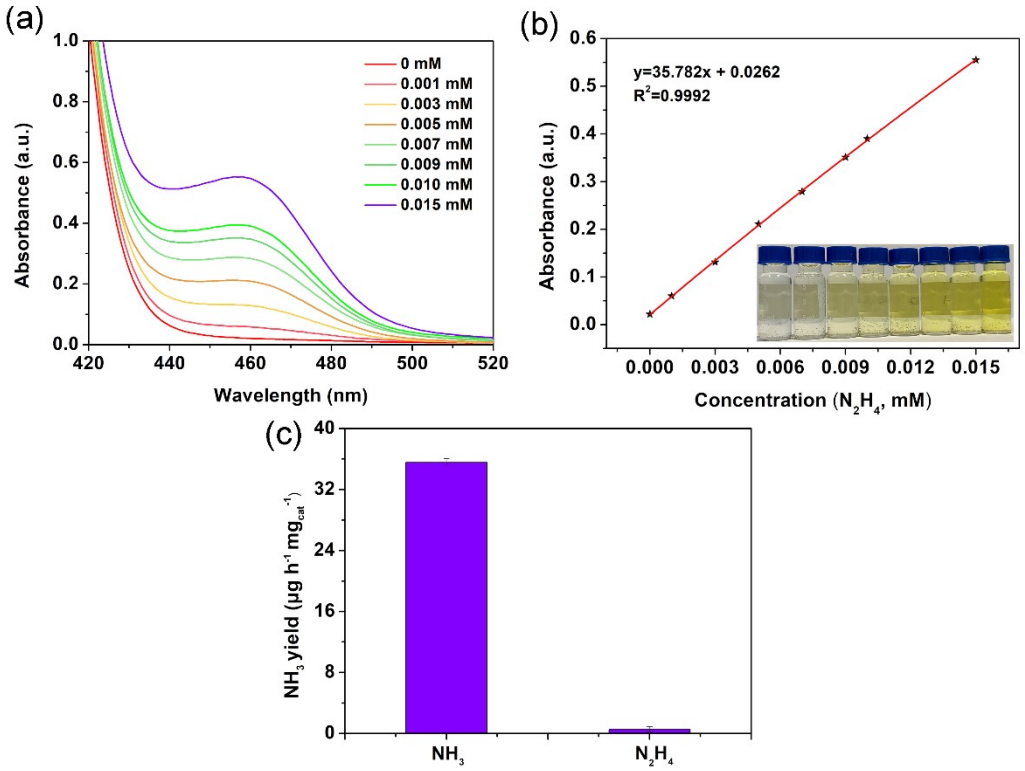

Fig. S19 (a) UV-vis colorimetric spectra of various concentrations of N_2H_4 using Watt and Chrisp method. (b) The standard curve used for assessment of N_2H_4 concentrations. (c) The yield of NH_3 and N_2H_4.

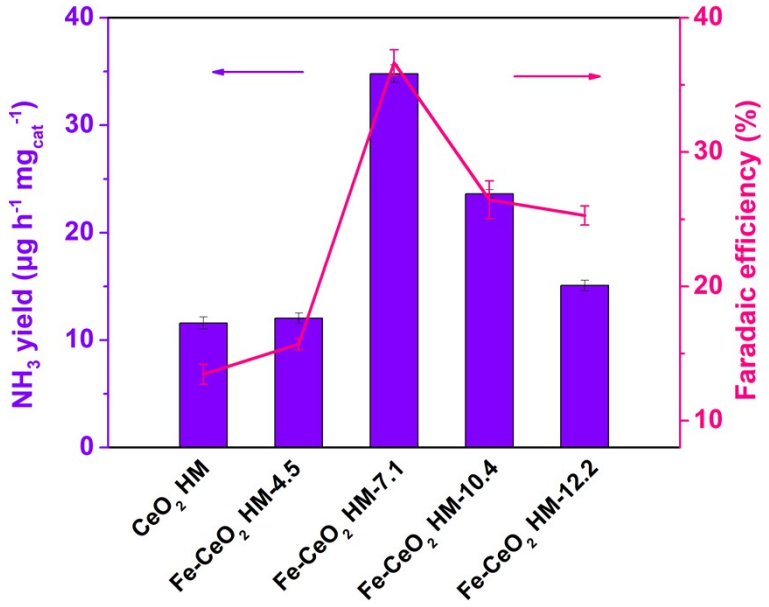

Fig. S20 NRR performance of different electrocatalysts obtained at –0.4 V.

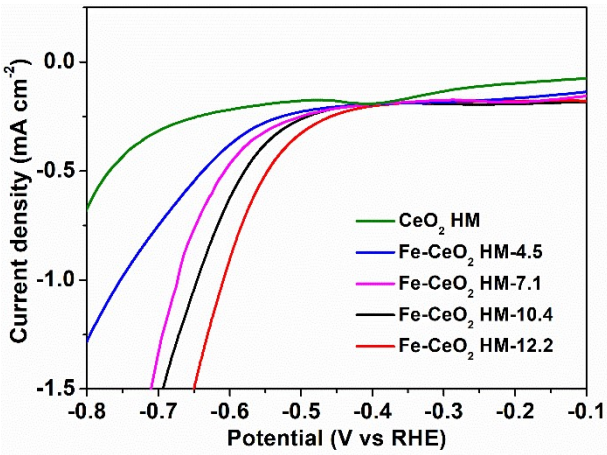

Fig. S21 LSV curves of CeO_2 HM and Fe doped CeO_2 HM with different Fe doping mass ratios in Ar-saturated 0.1 M Na_2SO_4 solution.

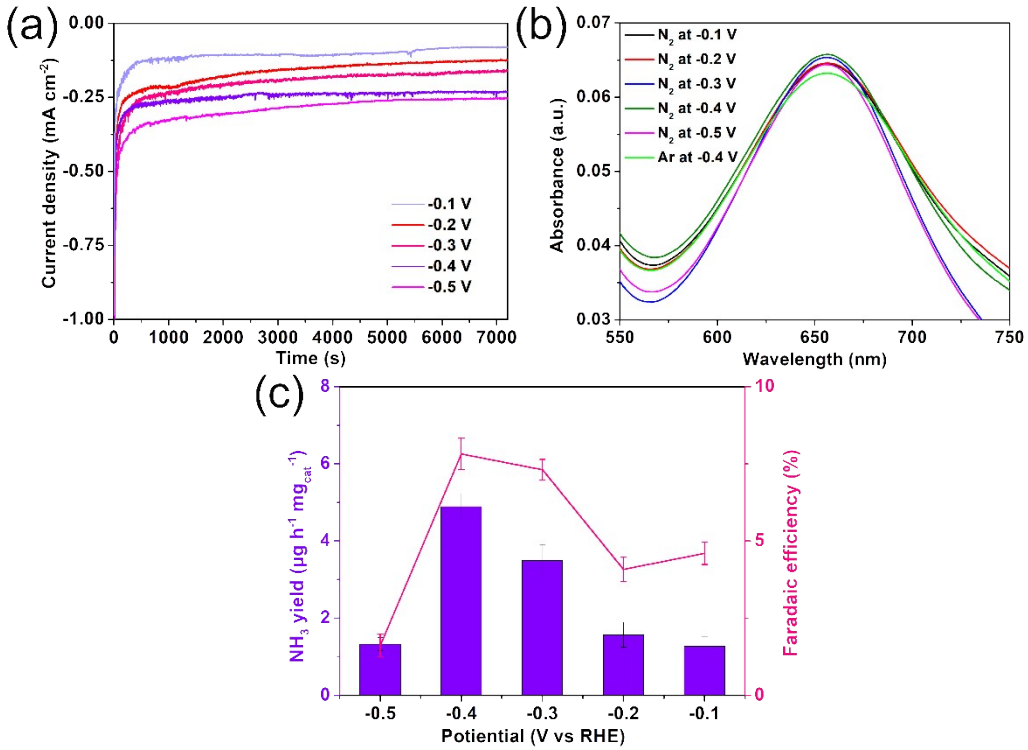

Fig. S22 NRR performance of CeO_2 HM-Precursor. (a) Time-dependent current density curves for CeO_2 HM-Precursor at each given potential. (b) UV-vis colorimetric spectra of N_2-saturated electrolytes stained by indophenol blue indicator after 2 h electrolysis at respective potentials and Ar-saturated electrolytes stained by indophenol blue indicator after 2 h electrolysis at -0.4 V. (c) The comparison of ammonia yield and faraday efficiency at different potentials.

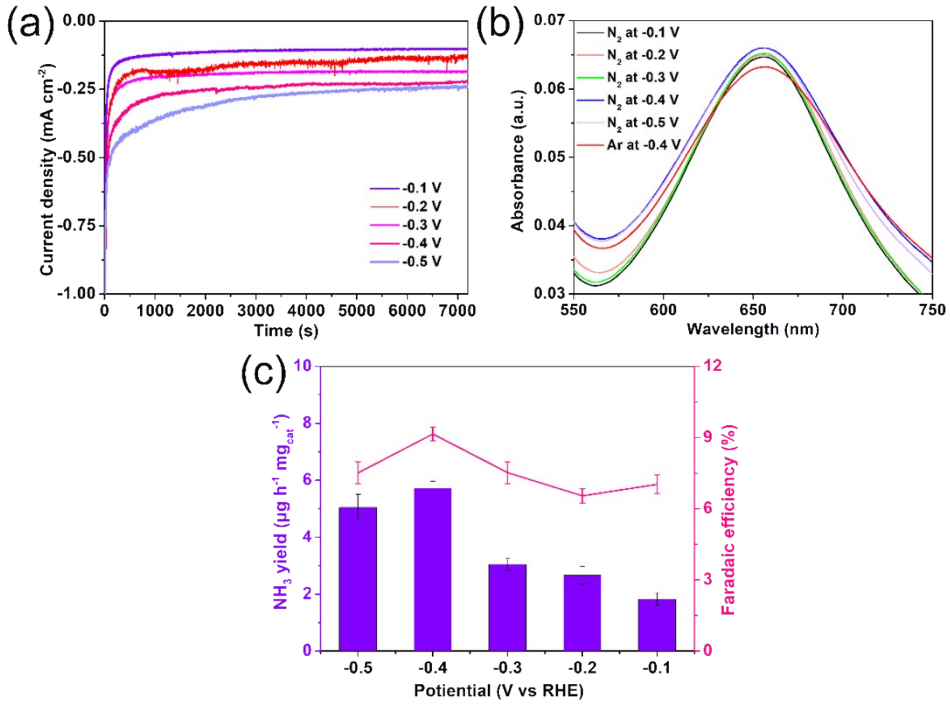

Fig. S23 NRR performance of Fe-CeO_2 HM-Precursor. (a) Time-dependent current density curves for Fe-CeO_2 HM-Precursor at each given potential. (b) UV-vis colorimetric spectra of N_2-saturated electrolytes stained by indophenol blue indicator after 2 h electrolysis at respective potentials and Ar-saturated electrolytes stained by indophenol blue indicator after 2 h electrolysis at -0.4 V. (c) The comparison of ammonia yield and faraday efficiency at different potentials.

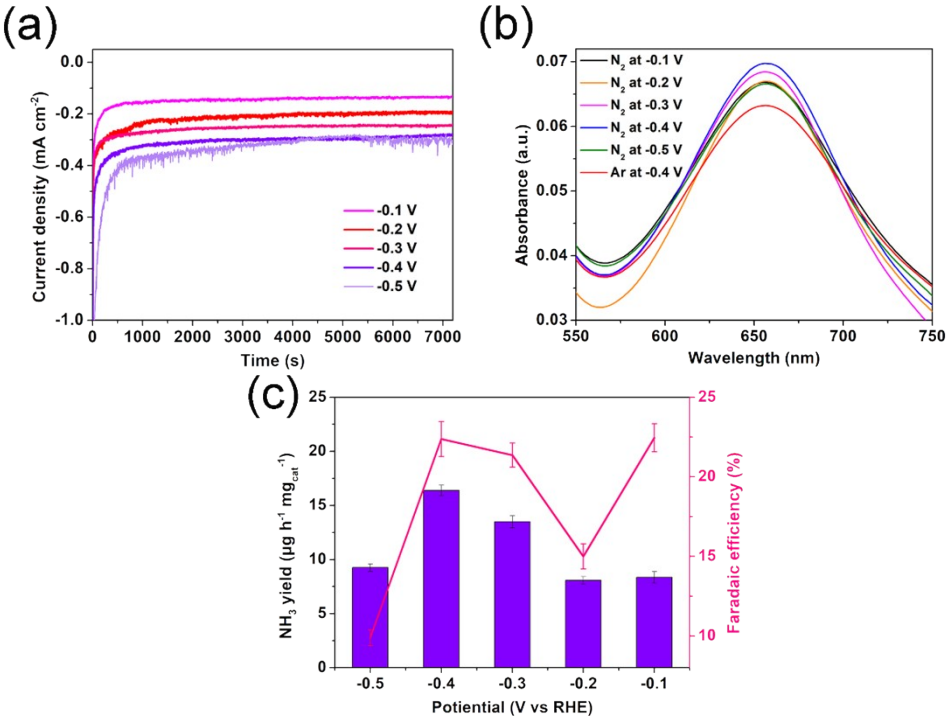

Fig. S24 NRR performance of Fe-CeO_2 NR. (a) Time-dependent current density curves for Fe-CeO_2 NR at each given potential. (b) UV-vis colorimetric spectra of N_2-saturated electrolytes stained by indophenol blue indicator after 2 h electrolysis at respective potentials and Ar-saturated electrolytes stained by indophenol blue indicator after 2 h electrolysis at -0.4 V. (c) The comparison of ammonia yield and faraday efficiency at different potentials.

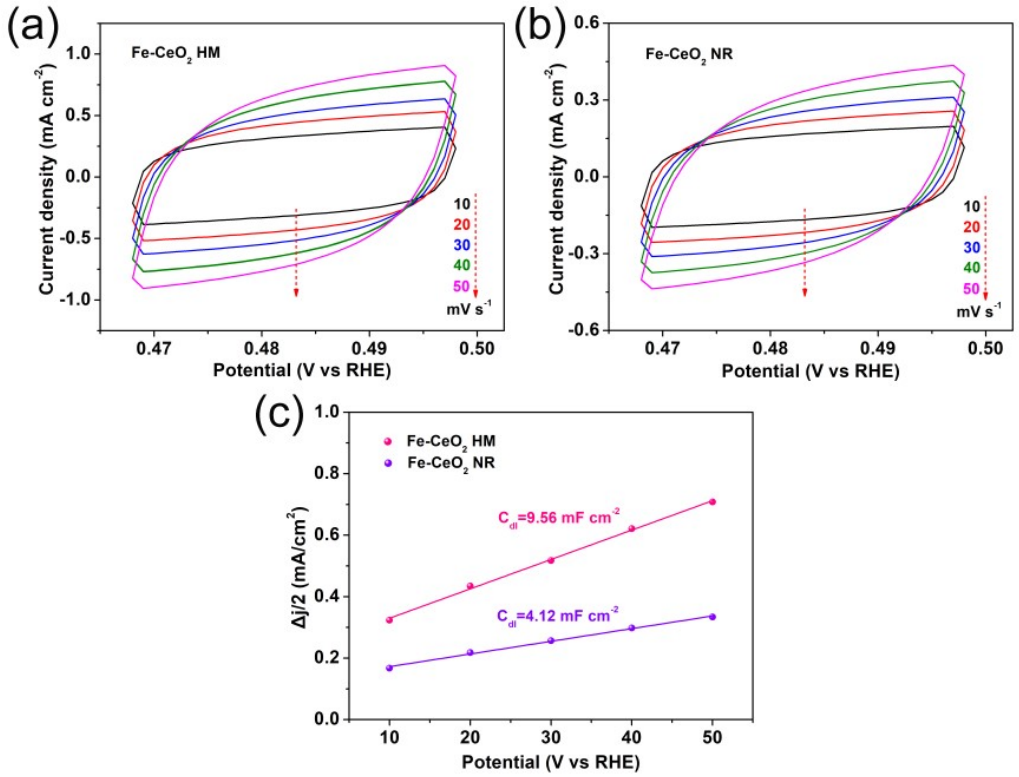

Fig. S25 (a) CV curves at different scan rates within the non-Faradaic potential range for Fe-CeO_2 HM, (b) CV curves at different scan rates within the non-Faradaic potential range for Fe-CeO_2 RN, (C) Capacitive currents on the basis of scan rate for Fe-CeO_2 HM and Fe-CeO_2 NR.

The ECSA was determined assuming a general specific C_{dl} capacitance of 40 µF cm^{-2} for all samples

$$A_{ECSA}^{Fe-CeO_2\ HM} = \frac{9.56\ mF\ cm^{-2}}{40\ \mu F\ cm^{-2}\ per\ cm_{ECSA}^2} = 239\ cm_{ECSA}^2$$

$$A_{ECSA}^{Fe-CeO_2\ RN} = \frac{4.12\ mF\ cm^{-2}}{40\ \mu F\ cm^{-2}\ per\ cm_{ECSA}^2} = 103\ cm_{ECSA}^2$$

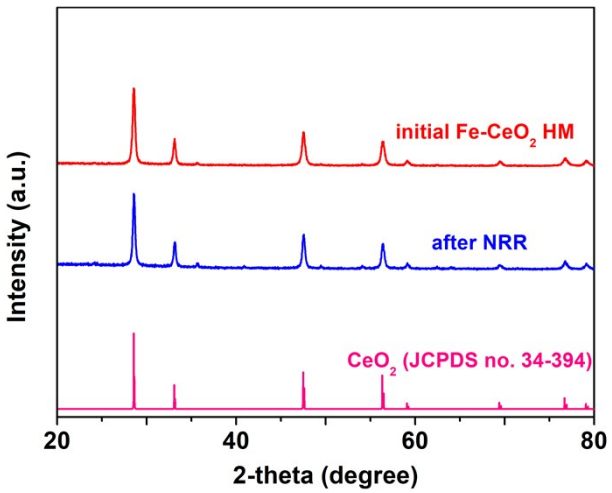

Fig. S26 XRD patterns of the Fe-CeO_2 HM before and after NRR stability tests.

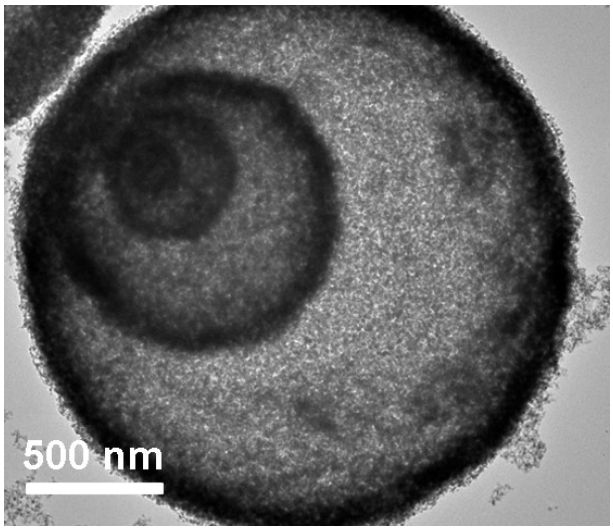

Fig. S27 TEM images of the Fe-CeO_2 HM after NRR stability tests.

Table S2. The NRR performance of Fe-CeO_2 HM comparing with other reported catalysts

Catalyst	Electrolyte	NH_3 yield	FE(%)
Fe_2O_3 nanorod[5]	0.1 M Na_2SO_4	15.9 μg h^{-1} mg^{-1}_{cat}	0.94%
γ-Fe_2O_3[6]	0.1 M KOH	0.212 μg h^{-1} mg^{-1}_{cat}	1.90%
β-FeOOH[7]	0.5 M $LiClO_4$	23.32 μg h^{-1} mg^{-1}_{cat}	6.70%
Fe/Fe_3O_4[8]	phosphate buffer solution	0.19 μg h^{-1} mg^{-1}_{cat}	8.29%
$Bi_4V_2O_{11}$/CeO_2[9]	0.1 M HCl	23.21 μg h^{-1} mg^{-1}_{cat}	10.16%
r-CeO_2 nanorod[10]	0.1 M Na_2SO_4	16.4 μg h^{-1} mg^{-1}_{cat}	3.70%
Fe-TiO_2[11]	0.5 M $LiClO_4$	25.47 μg h^{-1} mg^{-1}_{cat}	25.60%
CeO_2 rGO[12]	0.1 M Na_2SO_4	16.98 μg h^{-1} mg^{-1}_{cat}	4.78%

$FeMoO_4$[13]	0.1 M Na_2SO_4	17.51 μg h^{-1} mg^{-1}_{cat}	10.50%
FeSA-NO-C-900[14]	0.1 M HCl	31.9 μg h^{-1} mg^{-1}_{cat}	11.80%
OV-rich a-Fe_2O_3[15]	0.1 M KOH	32.13 μg h^{-1} mg^{-1}_{cat}	6.63%
Fe_{SA}-N-C[16]	0.1 M KOH	7.48 μg h^{-1} mg^{-1}_{cat}	56.55%
Ru/CeO_2-Vo[17]	0.05 M H_2SO_4	9.87×10^{-8} mmol·s^{-1}·cm^{-2}	11.70%
$Cr_{0.1}CeO_2$[1]	0.1 M Na_2SO_4	16.82μg h^{-1} mg^{-1}_{cat}	3.84%
Cu-CeO_2-3.9[18]	0.1 M Na_2SO_4	5.3×10^{-10} mol cm^{-2} s^{-1}	19.10%
MnO_x NA/TM[19]	0.1 M Na_2SO_4	1.63×10^{-10} mol cm^{-2} s^{-1}	11.40%
CuS-CPSs[20]	0.1 M HCl	18.18 μg h^{-1} mg^{-1}_{cat}	5.63%
$LiFe_5O_8$–rGO/CP[21]	0.1 M HCl	36.025 μg h^{-1} mg^{-1}_{cat}	13.08%
FeSAs-MoS_2[22]	0.5 M K_2SO_4 (pH = 3)	8.63 μg h^{-1} mg^{-1}_{cat}	18.80%
mRhRu/NF[23]	0.1 M Na_2SO_4	30.28 μg h^{-1} mg^{-1}_{cat}	28.33%
CeP–rGO[24]	0.1 M HCl	28.69 μg h^{-1} mg^{-1}_{cat}	9.60%
Fe_2O_3-rGO[25]	0.5 M $LiClO_4$	22.13 μg h^{-1} mg^{-1}_{cat}	5.89%
MnO/TM[26]	0.1 M Na_2SO_4	7.92 μg h^{-1} mg^{-1}_{cat}	8.02%
Fe_2O_3-CNT[27]	$KHCO_3$	0.22 μg h^{-1} cm^{-2}	0.15%
30% Fe_2O_3-CNT[28]	0.5 M KOH	0.52 μg h^{-1} cm^{-2}	0.16%
Fe_3O_4/Ti[29]	0.1 M Na_2SO_4	5.6×10^{-11} mol $s^{-1}cm^{-2}$	2.60%
Fe-CeO_2 HM[this work]	**0.1 M Na_2SO_4**	**34.79 μg h^{-1} mg^{-1}_{cat}**	**36.66%**

References

1 H. Xie, H. Wang, Q. Geng, Z. Xing, W. Wang, J. Chen, L. Ji, L. Chang, Z. Wang and J. Mao, Oxygen vacancies of Cr-doped CeO_2 nanorods that efficiently enhance the performance of electrocatalytic N_2 fixation to NH_3 under ambient conditions, *Inorg. Chem*., 2019, **58**, 5423-5427.

2 L. Li, C. Tang, B. Xia, H. Jin, Y. Zheng and S.-Z. Qiao, Two-dimensional mosaic bismuth nanosheets for highly selective ambient electrocatalytic nitrogen reduction, *ACS Catal.,* 2019, **9**, 2902-2908.

3 F. Pang, Z. Wang, K. Zhang, J. He, W. Zhang, C. Guo and Y. Ding, Bimodal nanoporous Pd_3Cu_1 alloy with restrained hydrogen evolution for stable and high yield electrochemical nitrogen reduction, *Nano Energy*., 2019, **58**, 834-841.

4 Y. C. Hao, Y. Guo, L. W. Chen, M. Shu, X. Y. Wang, T. A. Bu, W. Y. Gao, N. Zhang, X. Su, X. Feng, J. W. Zhou, B. Wang, C. W. Hu, A. X. Yin, R. Si, Y. W. Zhang and C. H. Yan, Promoting nitrogen electroreduction to ammonia with bismuth nanocrystals and potassium cations in water, *Nat Catal*., 2019, **2**, 448-456.

5 X. Xiang, Z. Wang, X. Shi, M. Fan and X. Sun, Ammonia synthesis from electrocatalytic N_2 reduction under ambient conditions by Fe_2O_3 nanorods, *ChemCatChem*, 2018, **10**, 4530-4535.

6 J. Kong, A. Lim, C. Yoon, J. H. Jang, H. C. Ham, J. Han, S. Nam, D. Kim, Y. E. Sung, J. Choi and H. S. Park, Electrochemical synthesis of NH_3 at low temperature and atmospheric pressure using a γ-Fe_2O_3 catalyst, *ACS Sustainable Chem. Eng*., 2017, **5**, 10986-10995.

7 X. Zhu, Z. Liu, Q. Liu, Y. Luo, X. Shi, A. M. Asiri, Y. Wu and X. Sun, Efficient and durable N_2 reduction electrocatalysis under ambient conditions: β-FeOOH nanorods as a non-noble-metal catalyst, *Chem. Commun.,* 2018, **54**, 11332-11335.

8 C. Li, Y. Fu, Z. Wu, J. Xia and X. Wang, Ambient electrochemical ammonia synthesis with high selectivity on Fe/Fe-oxide catalyst, *ACS Catal.,* 2018, **8**, 9312-9319.

9 C. Lv, C. Yan, G. Chen, Y. Ding, J. Sun, Y. Zhou and G. Yu, An amorphous noble-metal-free electrocatalyst that enables nitrogen fixation under ambient conditions, *Angew. Chem. Int. Ed*., 2018, **57**, 6073-6076.

10 B. Xu, L. Xia, F. Zhou, R. Zhao, H. Chen, T. Wang, Q. Zhou, Q. Liu, G. Cui, X. Xiong, F. Gong and X. Sun, Enhancing electrocatalytic N_2 reduction to NH_3 by CeO_2 nanorod with oxygen vacancies, *ACS Sustainable Chem. Eng*., 2019, **7**, 2889-2893.

11 T. Wu, X. Zhu, Z. Xing, S. Mou, C. Li, Y. Qiao, Q. Liu, Y. Luo, X. Shi, Y. Zhang and X. Sun, Greatly improving electrochemical N_2 reduction over TiO_2 nanoparticles by iron doping, *Angew. Chem. Int. Ed*., 2019, **58**, 18449-18453.

12 H. Xie, Q. Geng, X. Li, T. Wang, Y. Luo, A. A. Alshehri, K. A. Alzahrani, B. Li, Z. Wang and J. Mao, Ceria-reduced graphene oxide nanocomposite as an efficient electrocatalyst towards artificial N_2 conversion to NH_3 under ambient conditions, *Chem. Commun*., 2019, **55**, 10717-10720.

13 J. Wu, Z. Wang, S. Li, S. Niu, Y. Zhang, J. Hu, J. Zhao and P. Xu, $FeMoO_4$ nanorods for efficient ambient electrochemical nitrogen reduction, *Chem. Commun*., 2020, **56**, 6834-6837.

14 Y. Li, J. Li, J. Huang, J. Chen, Y. Kong, B. Yang, Z. Li, L. Lei, G. Chai, Z. Wen, L. Dai and Y. Hou, Boosting electroreduction kinetics of nitrogen to ammonia via tuning electron distribution of single-atomic iron sites, *Angew. Chem. Int. Ed*., 2021, **60**, 9078-9085.

15 C. Zhang, S. Liu, T. Chen, Z. Li and J. Hao, Oxygen vacancy-engineered Fe_2O_3 nanocubes via a task-specific ionic liquid for electrocatalytic N_2 fixation, *Chem. Commun*., 2019, **55**, 7370-7373.

16 M. Wang, S. Liu, T. Qian, J. Liu, J. Zhou, H. Ji, J. Xiong, J. Zhong and C. Yan, Over 56.55% faradaic efficiency of ambient ammonia synthesis enabled by positively shifting the reaction potential, *Nat. Commun*., 2019, **10**, 341.

17 Y. Ding, L. Huang, J. Zhang, A. Guan, Q. Wang, L. Qian, L. Zhang and G. Zheng, Ru-doped, oxygen-vacancy-containing CeO_2 nanorods toward N_2 electroreduction, *J. Mater. Chem. A*, 2020, **8**, 7229-7234.

18 S. Zhang, C. Zhao, Y. Liu, W. Li, J. Wang, G. Wang, Y. Zhang, H. Zhang and H. Zhao, Cu doping in CeO_2 to form multiple oxygen vacancies for dramatically enhanced ambient N_2 reduction performance, *Chem. Commun*., 2019, **55**, 2952-2955.

19 L. Zhang, X.- Y. Xie, H. Wang, L. Ji, Y. Zhang, H. Chen, T. Li, Y. Luo, G. Cui and X. Sun, Boosting electrocatalytic N_2 reduction by MnO_2 with oxygen vacancies, *Chem. Commun*., 2019, **55**, 4627-4630.

20. S. Li, Y. Wu, Q. Liu, B. Li, T. Li, H. Zhao, A. A. Alshehri, K. A. Alzahrani, Y. Luo, L. Li and X. Sun, CuS concave polyhedral superstructures enabled efficient N_2 electroreduction to NH_3 at ambient conditions, *Inorg. Chem. Front*., 2021, **8**, 3105-3110.

21 Y. Ji, L. Li, W. Cheng, Y. Xiao, C. Li and X. Liu, Electrochemical N_2 fixation to NH_3 under ambient conditions: porous $LiFe_5O_8$ nanoparticle–reduced graphene oxide as a highly efficient and selective catalyst, *Inorg. Chem. Front*., 2021, **8**, 3156-3161.

22. H. Su, L. Chen, Y. Chen, R. Si, Y. Wu, X. Wu, Z. Geng, W. Zhang and J. Zeng, Single atoms of iron on MoS_2 nanosheets for N_2 electroreduction into ammonia, *Angew. Chem. Int. Ed*., 2020, **59**, 20411-20416.

23. Z. Wang, W. Tian, Z. Dai, T. Zhou, Q. Mao, Y. Xu, X. Li, L. Wang and H. Wang, Bimetallic mesoporous RhRu film for electrocatalytic nitrogen reduction to ammonia, *Inorg. Chem. Front*., 2021, **8**, 4276-4281.

24. Y. Ji, L. Li, W. Cheng, Y. Xiao, C. L and X. Liu, A CeP nanoparticle-reduced graphene oxide hybrid: an efficient electrocatalyst for the NH_3 synthesis under ambient conditions, *Inorg. Chem. Front*., 2021, **8**, 2103-2106.

25. J. Li, X. Zhu, T. Wang, Y. Luo and X. Sun, An Fe_2O_3 nanoparticle-reduced graphene oxide composite for ambient electrocatalytic N_2 reduction to NH_3, *Inorg. Chem. Front*., 2019, **6**, 2682-2685.

26. Z. Wang, F. Gong, L. Zhang, R. Wang, L. Ji, Q. Liu, Y. Luo, H. Guo, Y. Li, P. Gao, X. Shi, B. Li, B. Tang and X. Sun, Electrocatalytic hydrogenation of N_2 to NH_3 by MnO: experimental and theoretical investigations, *Adv. Sci*., 2019, **6**, 1801182-1801190.

27 S. Chen, S. Perathoner, C. Ampelli, C. Mebrahtu, D. Su and G. Centi, Electrocatalytic synthesis of ammonia at room temperature and atmospheric pressure from water and nitrogen on a carbon-nanotube-based electrocatalyst, *Angew. Chem. Int. Ed*., 2017, **56**, 2699-2703.

28 S. Chen, S. Perathoner, C. Ampelli, C. Mebrahtu, D. Su and G. Centi, Room-Temperature electrocatalytic synthesis of NH_3 from H_2O and N_2 in a gas–liquid–solid three-phase reactor, *ACS Sustainable Chem. Eng*., 2017, **5**, 7393-7400.

29 Q. Liu, X. Zhang, B. Zhang, Y. Luo, G. Cui, F. Xie and X. Sun, Ambient N_2 fixation to NH_3 electrocatalyzed by a spinel Fe_3O_4 nanorod, *Nanoscale*, 2018, **10**, 14386-14389.